Supplementary Section 1: Polarized Raman Spectra of $MoOCl_2$ and $NbOCl_2$

Fig. S1a and S1b present the polarized Raman spectra of $MoOCl_2$ and $NbOCl_2$, respectively. For $MoOCl_2$[1] (Fig. S1a), five prominent Raman active modes are observed within the wavenumber range of 100 to 600 cm^{-1}. Specifically, the B_g mode at approximately 123 cm^{-1} corresponds to the out-of-phase shear-slip motion of the dimerized Mo-O chains along the x-axis. This mode exhibits a characteristic $\sin^2 2\theta$ four-lobed polarization dependence, serving as an intrinsic marker for identifying the crystallographic orientation. The A_g symmetry mode near 177 cm^{-1} originates from the collective out-of-phase breathing vibration of the Mo-Cl-Mo-Cl units. This mode represents the most significant electron-phonon coupling: it exhibits a distinct asymmetric Fano lineshape when excited along the metallic x-axis, while reverting to a nearly Lorentzian profile along the y-axis, reflecting the strong coupling between phonons and the quasi-one-dimensional (1D) metallic electronic continuum.Two additional A_g modes at approximately 289 cm^{-1} and 349 cm^{-1} correspond to the inter-chain and intra-chain breathing motions of the Mo-Cl-Mo-Cl units, respectively. The divergence in their polarization dependence clearly reveals the influence of electronic structural anisotropy on phonon self-energy renormalization. Notably, the 349 cm^{-1} mode is significantly enhanced under y-axis polarization and can be utilized alongside the 123 cm^{-1} peak to precisely determine the crystal orientation. The high-frequency A_g mode at 426 cm^{-1} primarily arises from the y-axis bending vibration of O atoms in the O–Mo–O chains. Its polarization behavior is consistent with the mid-frequency A_g modes and does not overlap with Raman peaks of common analytes, making it an ideal substrate internal standard. Overall, all A_g modes generally exhibit Fano asymmetry under x-axis excitation and symmetric lineshapes under y-axis excitation, confirming that Fano resonance is an intrinsic signature of the quasi-1D metallic channels in $MoOCl_2$.

The $NbOCl_2$ [2–4]crystal belongs to the C_2 space group with 8 atoms in its primitive cell, corresponding to 24 phonon vibrational modes (11A + 10B Raman-active modes according to the irreducible representation). As shown in Fig. S1b, four primary Raman peaks are identified within the 100-600cm^{-1} range. In the low-frequency region (~160-180 cm^{-1}), the peaks stem from Nb-O related in-plane vibrations. The characteristic peak at ~156 cm^{-1} corresponds to the in-plane shear vibration of Nb and O atoms, where atomic displacements are confined within the Nb-O framework with negligible interlayer coupling. The intense peak at ~175 cm^{-1} is dominated by the in-plane bending vibration of O atoms, representing one of the strongest Raman-active modes in $NbOCl_2$. The mode at ~296 cm^{-1} involves the synergistic in-plane vibration of Cl and Nb atoms along the principal axes. The peak near 340 cm^{-1} is attributed to the in-plane stretching vibration of the Nb-O-Cl bonds. The Raman response of $NbOCl_2$ is dominated by A-symmetry modes, exhibiting pronounced in-plane anisotropy. All peaks satisfy the polarization dependence of A-symmetry modes: a periodicity of π under parallel polarization and a $\sin^2 2\theta$dependence under cross-polarization, without the $\pi/2$ periodicity characteristic of B-symmetry modes, consistent with the C_2 symmetry of $NbOCl_2$.

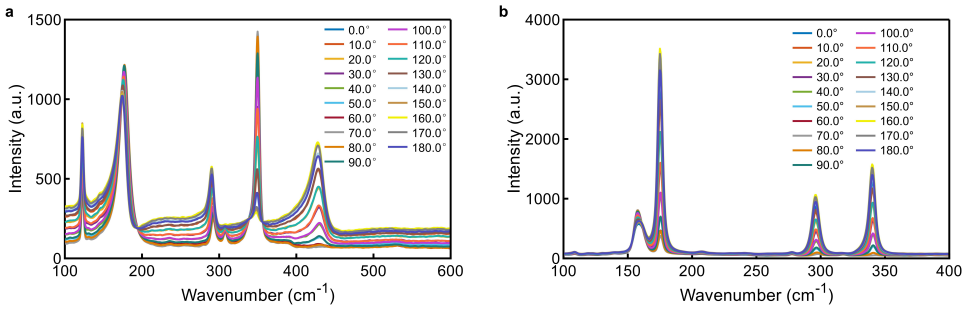

Fig. S1. Polarization-resolved Raman spectra of (a) $MoOCl_2$ and (b) $NbOCl_2$.

Supplementary Section 2: Theoretical Calculations for $MoOCl_2$ and $NbOCl_2$

Figure S2a illustrates the optical loss characteristics of $MoOCl_2$ along the in-plane x and y-axes. The optical loss can be characterized by the absorption coefficient α, which is related to the imaginary part of the refractive index κ and the incident wavelength λ by the following expression:

$$\alpha = \frac{4\pi\kappa}{\lambda}$$

As shown in Fig. S2a, $MoOCl_2$ exhibits significantly higher optical loss along the x-axis compared to the y-axis within the visible spectrum, demonstrating strong in-plane anisotropic absorption. This property enables $MoOCl_2$ to act as an effective ultrathin linear polarizer by differentially absorbing light of different polarization states.

Furthermore, based on the theoretical formula for phase retardation:

$$d = m\lambda/4\Delta n$$

we calculated the required thickness d for $NbOCl_2$ to function as a QWP across the 360-1500 nm range (Fig. S2b), where Δn is the in-plane birefringence and λ is the incident wavelength. The results indicate that $NbOCl_2$ possesses substantial in-plane refractive index anisotropy, allowing it to satisfy the QWP condition at nanometer-scale thicknesses. This not only drastically reduces the thickness requirements of conventional waveplates but also provides a foundation for ultrathin, broadband on-chip polarization control devices.

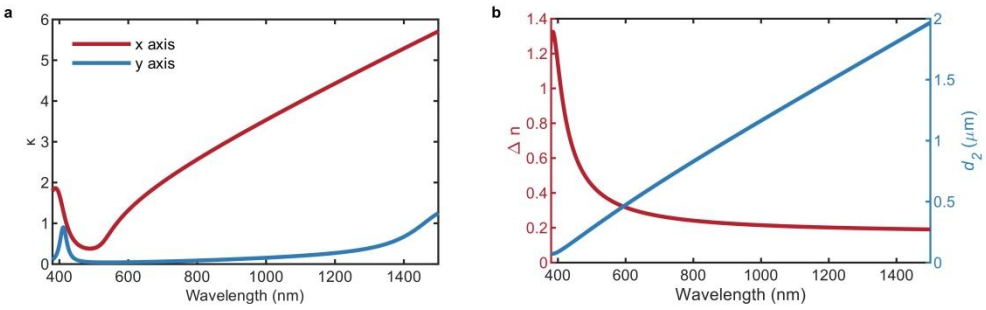

Fig. S2. (a) Optical loss coefficient κ of $MoOCl_2$ as a function of the incident wavelength λ along the in-plane x- and y-axis directions. (b) Wavelength dependence of the birefringence Δn between the two orthogonal in-plane principal axes of $NbOCl_2$ (left axis) and the required thickness for $NbOCl_2$ to function as a quarter-wave plate (right axis).

Supplementary Section 3: Determination of the Relative Orientation of Stacked Structures

Fig. S3a-c show the simulated T_{LCP}/T_{RCP} ratios as a function of twist angle and wavelength for three thickness combinations: (a) 380nm $MoOCl_2$/310nm $NbOCl_2$, (b) 300nm $MoOCl_2$/650nm $NbOCl_2$, and (c) 600nm $MoOCl_2$/200nm $NbOCl_2$.

To investigate the influence of the relative orientation between $MoOCl_2$ and $NbOCl_2$ on polarization selectivity, we analyzed the device performance across the 0° to 90° twist angle range. Across all combinations, a distinct optimal twist angle exists at specific wavelengths where the device achieves maximum circular polarization contrast or specific transmission extrema. The optimal angle varies with the thicknesses of the individual layers. This thickness dependence arises because $MoOCl_2$ and $NbOCl_2$, as anisotropic van der Waals crystals, accumulate different amounts of phase retardation due to their intrinsic birefringence and dichroism. Consequently, the twist angle between the crystallographic axes must be precisely tuned to match the polarization conversion conditions for compensating or enhancing specific circular polarization states.

For the 380nm $MoOCl_2$/310nm $NbOCl_2$ stack, an optimal twist angle of approximately 48° is identified at 553.3 nm, yielding the most efficient polarization selectivity. This provides critical parameter guidance for the development of high-performance, ultrathin, lithography-free circular polarization filters.

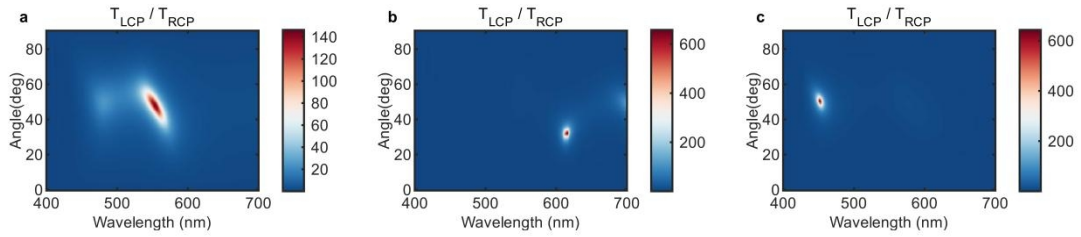

Fig. S3. Simulated T_{LCP}/T_{RCP} ratios as a function of twist angle and wavelength for three thickness combinations: (a) 380 nm $MoOCl_2$ / 310 nm $NbOCl_2$, (b) 300 nm $MoOCl_2$ / 650 nm $NbOCl_2$, and (c) 600 nm $MoOCl_2$ / 200 nm $NbOCl_2$.

Supplementary Section 4: Transmission Ratio as a Function of Thickness in Stacked Structures

Figure S4 provides a detailed mapping of the stacked transmission ratio as a function of layer thicknesses with fine steps.

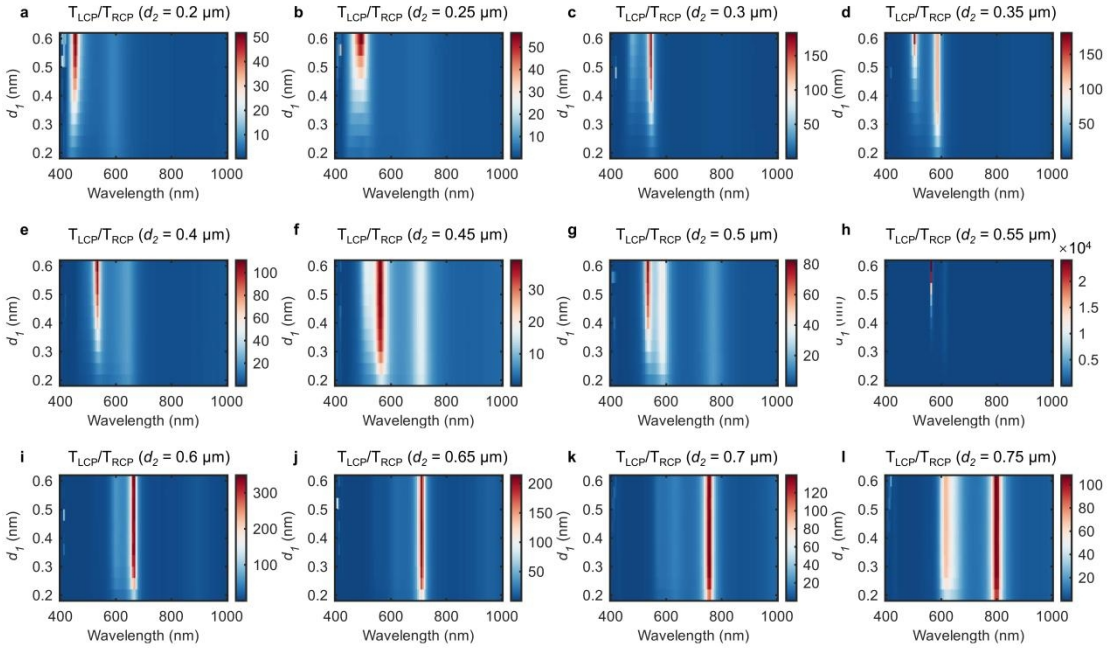

Fig. S4. Transmission ratios of LCP and RCP after passing through $MoOCl_2/NbOCl_2$ stacked structures with different thickness combinations.

Supplementary Section 5: Comparison between Experimental and Simulated Transmission Spectra

Figure S5 presents the comparison between experimental results and FDTD simulations. Fig. S5a and S5b show the transmission curves of 380 nm $MoOCl_2$ in the visible range (400-700 nm) under x- and y-polarized light, respectively (blue solid lines: experiment; red dashed lines: simulation). The theoretical data are in good agreement with the experimental results. Under x-polarization, both spectra exhibit a peak within the 400-500 nm band (Fig. S5a). Under y-polarization, both show two characteristic peaks within the 500-700 nm band. The slightly higher experimental transmission compared to simulation under x-polarization may stem from the non-ideal linearity of the polarizer in the experimental setup. Figure S5c compares the T_y/T_x ratios; although the experimental values are lower than the simulation, an extinction ratio of nearly 20 dB is maintained in the 600-700 nm range.

Fig. S5d and S5e display the transmission spectra for 310 nm $NbOCl_2$ with the output polarizer oriented along the x and y directions, respectively. The data match well in the x direction (Fig. S5d), with both showing a small peak near 450 nm. A redshift is observed in the experimental peak for the y direction (Fig. S5e), potentially due to discrepancies in the material's dielectric constants or thicknesses used in the simulation, or non-ideality in the circular polarization of the light source. Figure S5f shows the ratio of T_y/T_x for $NbOCl_2$, confirming that $NbOCl_2$ of a specific thickness can exhibit excellent quarter-wave plate characteristics at targeted wavelengths.

Figs. S5g–i compare the experimental data with numerical simulations for $MoOCl_2$/ $NbOCl_2$ stacked structure. The experimental curves show excellent agreement with the simulated trends. Minor discrepancies at the boundaries (400 nm and 700 nm) are likely due to the decreased circularity of the polarizers at the edge of their working bandwidth. The slight redshift in the T_{LCP} peak compared to simulation may stem from differences in the refractive index between the actual sample and the idealized model.

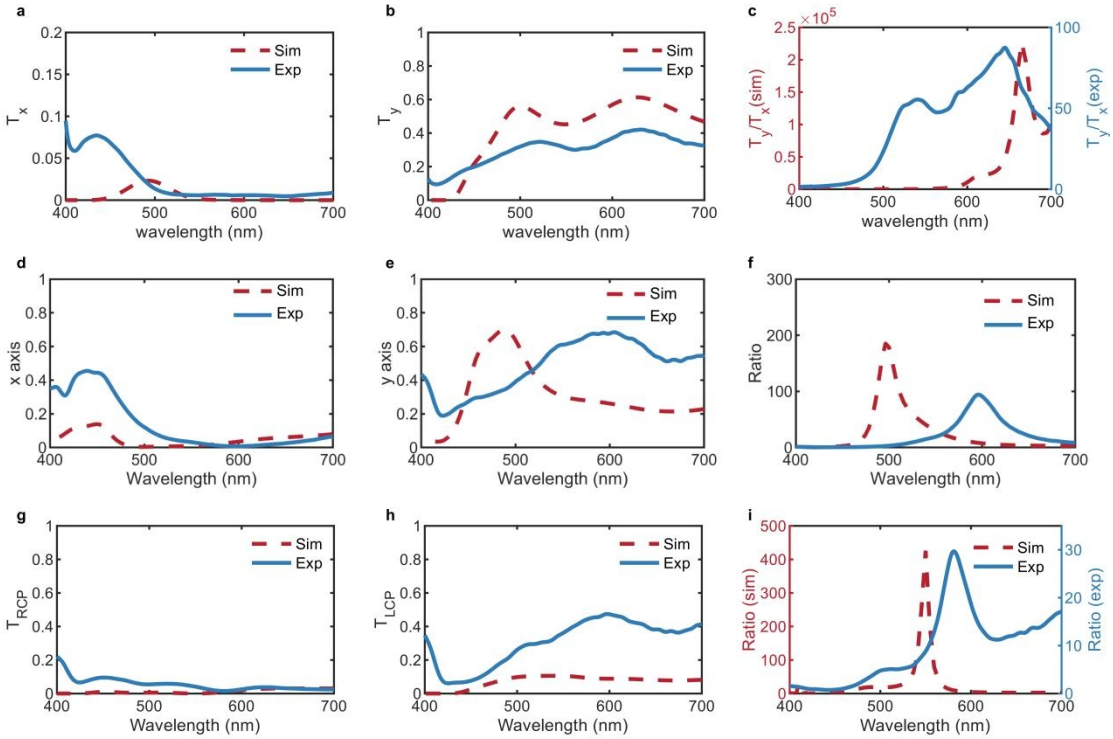

Fig. S5. Comparison between experimental and simulated transmission spectra. The blue solid lines represent the experimental results, while the red dashed lines represent the simulated results. (a, b) Experimental and simulated transmission spectra of a 380 nm $MoOCl_2$ flake in the visible range (400–700 nm) under x-polarized (a) and y-polarized (b) illumination. (c) Comparison between the experimental (right axis) and simulated (left axis) T_y/T_xratios of the 380 nm $MoOCl_2$ sample. (d, e) Experimental and simulated transmission spectra of a 310 nm $NbOCl_2$ sample in the visible range (400–700 nm) with the analyzer in the output path aligned along the x (d) and y (e) directions. (f) Ratio of the transmission with the analyzer aligned along the y direction to that along the x direction for the 310 nm $NbOCl_2$ sample, comparing experimental and simulated results. (g, h) Experimental and simulated transmission spectra of the stacked structure under LCP (g) and RCP (h) incidence, with the insets showing the corresponding optical micrographs. (i) Comparison between the experimental (right axis) and simulated (left axis) transmission ratios $T_{LCP}/T_{RCP}$of the $MoOCl_2$/$NbOCl_2$ stacked structure in the visible spectral range.

Supplementary Section 6: Stability of the $MoOCl_2$/ $NbOCl_2$ stacked structure

Figure S6a (corresponding to Fig. 3l) shows the T_{LCP}/T_{RCP} measured immediately after fabrication, while Figure S6b shows the data after six months of ambient exposure. The T_{LCP}/T_{RCP} ratio remains as high as 25.51, representing a minimal decrease of only 14%. This demonstrates the excellent environmental stability of the developed stacked structures.

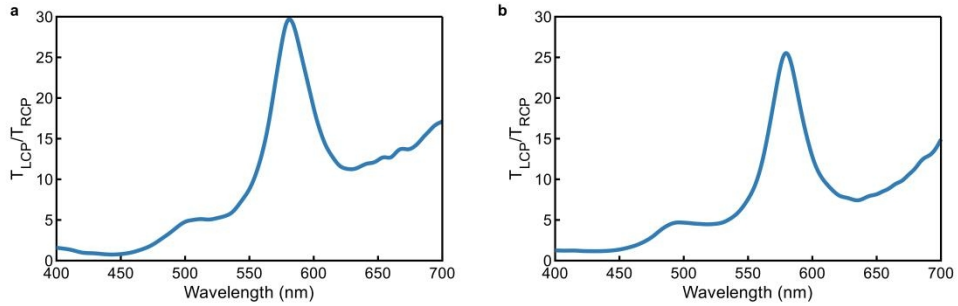

Fig. S6. Stability of the $MoOCl_2/NbOCl_2$ stacked structure. (a) T_{LCP}/T_{RCP} measured immediately after fabrication. (b) T_{LCP}/T_{RCP} after six months of ambient exposure.

References

1. Minnekhanov, A. *et al.* Hyperbolic-enhanced Raman scattering in van der Waals $MoOCl_2$: from Fano resonances to picomolar detection.

2. Xu, M. *et al.* Twist angle dependent high degree of anisotropic emission and phonon scattering in WS_2 /$NbOCl_2$ heterostructures. *Nanoscale* **17**, 6079–6089 (2025).

3. Guo, Q. *et al.* Ultrathin quantum light source with van der Waals NbOCl2 crystal. *Nature* **613**, 53–59 (2023).

4. Wang, Y., Wu, Y. & Sun, M. Indirect and direct electronic transitions and electron transport properties of van der Waals $NbOCl_2$. *Phys. Chem. Chem. Phys.* **26**, 22518–22528 (2024).